Eurasian Chem.-Technol. J. 27 (2025) 191–198
The journal of the Institute of Combustion Problems https://ect-journal.kz

https://doi.org/10.18321/ectj1666

Synthesis of a Bimetallic Co/Zn Zeolitic Imidazolate Framework-C_{60} Fullerene Nanowhisker Composite and its Photocatalytic Degradation of Tetracycline Hydrochloride under LED Light Condition

Seung Won Ko, and Hoon Chung*

Department of Convergence Science, Graduate School, Sahmyook University, 815, Seoul 139-742, South Korea

Article info

Received:
12 May 2025

Received in revised form:
25 June 2025

Accepted:
13 August 2025

Keywords:
Co/Zn-ZIF-C_{60} FNW composite;
Photocatalytic activity;
Tetracycline hydrochloride;
LED light irradiation;
Pseudo-first-order rate law

Abstract

Bimetallic Co/Zn zeolitic imidazolate framework (Co/Zn-ZIF) nanoparticles were prepared via a simple process involving the dissolution of cobalt nitrate hexahydrate ($Co(NO_3)_2{\cdot}6H_2O$), zinc nitrate hexahydrate ($Zn(NO_3)_2{\cdot}6H_2O$), and 2-methylimidazole ($C_4H_6N_2$) in methanol (CH_3OH) with stirring at 25 °C for 2 h. The resulting solid-state Co/Zn ZIF nanoparticles are collected by centrifugation and dried at 60 °C for 24 h. C_{60} fullerene nanowhiskers (FNW) were prepared from C_{60}-saturated toluene and isopropyl alcohol using a liquid-liquid interfacial precipitation method. The composite was stirred while adding small amounts of solutions of polyvinylpyrrolidone (PVP, M_w ≈10,000 g/mol), C_{60} FNW, cobalt(II) nitrate hexahydrate, zinc nitrate hexahydrate, and 2-methylimidazole to afford bimetallic Co/Zn-ZIF-C_{60} FNW composite which is collected by centrifugation and dried for 24 h in an oven to obtain the bimetallic Co/Zn-ZIF-C_{60} FNW composite. The bimetallic Co/Zn-ZIF-C_{60} FNW composite exhibit higher photocatalytic activity than Co/Zn ZIF nanoparticles in the degradation of tetracycline hydrochloride (TCH) under LED light irradiation at 450 nm. The photocatalytic degradation kinetics of TCH in the presence of either Co/Zn ZIF nanoparticles or bimetallic Co/Zn-ZIF-C_{60} FNW composite under LED light irradiation followed a pseudo-first-order rate law.

1. Introduction

Recent industrial advancements have led to severe water contamination and thus cause significant harm to a crucial element of ecosystems [1] via the release of aquatic pollutants such as pesticides, polychlorinated biphenyls, fluorosurfactants, heavy metals, and pharmaceuticals [2]. Pharmaceuticals are particularly persistent pollutants in aquatic environments [3] because such compounds are designed to resist biological degradation. In addition to their poor biodegradation, trace amounts are commonly found in water bodies owing to their very low removal rates during water treatment processes [4, 5]. Moreover, the persistence of these substances in water poses a threat to aquatic ecosystems and potentially endangers human health [6].

Tetracycline is among the most widely produced and consumed antibiotic worldwide, primarily owing to its low toxicity and affordability [7, 8]. Pharmaceuticals are typically not fully absorbed by various organisms. In particular, approximately 35–90% of administered tetracycline is excreted and released into the ecosystem through various pathways, resulting in significant ecological threats, including the emergence of antibiotic-resistant bacteria and the potential development of new diseases [9]. Current water treatment facilities and conventional wastewater treatment processes fail to completely remove tetracycline: thus, additional economically viable and environmentally sustainable treatment methods are urgently required to effectively remove tetracycline from wastewater [10].

*Corresponding author.
E-mail address: larus@nate.com

Numerous studies have investigated the effectiveness of adsorption, membrane filtration, and advanced photocatalytic oxidation processes for the removal of antibiotics from wastewater [11-13]. Among these methods, adsorption-based techniques have garnered particularly significant attention owing to their cost-effectiveness, low energy consumption, operational simplicity, and environmental sustainability; however, the development of highly efficient and low-cost adsorbents remains a considerable challenge [14-17].

Metal-organic frameworks (MOFs) have recently emerged as promising adsorbents owing to their stable, porous structures and large specific surface areas; however, the large-scale application of MOFs is often limited by their instability in water. Recent studies have sought to address this issue by combining MOFs with carbon compounds generated during high-temperature carbonization processes, thereby improving their durability [18-20].

C_{60} fullerene nanowhiskers were prepared using a colloidal solution of lead zirconate containing C_{60} fullerene [21]. The nanowhiskers were synthesized via liquid-liquid interfacial precipitation (LLIP) and exhibited higher light transmittance and charge carrier mobility than pure C_{60} fullerene [22-24]. Furthermore, these materials have been used in various catalytic and photocatalytic applications [25-27]. Previous studies have employed C_{60} fullerene nanowhiskers for the photocatalytic degradation of organic dyes, including rhodamine B and methylene blue [28, 29].

In addition, the formation of secondary building units (SBUs) within the MOF structure enhances its performance relative to that of monophasic ZIF nanoparticles. Numerous studies have demonstrated that variations in the proportions of metal ions of bimetallic MOFs can alter the physicochemical properties of the materials [30, 31]. The catalytic activity of bimetallic MOFs in the degradation of tetracycline is superior to that of their monometallic counterparts [32].

Therefore, further research is required to investigate the application of these materials in the removal of trace pollutants, including antibiotics, from water. In this study, a nanocomposite incorporating C_{60} fullerene nanowhiskers and featuring a heterojunction structure (Co/Zn-ZIF-C_{60} FNW) was developed as a photocatalyst for the degradation of tetracycline hydrochloride under LED illumination.

2. Experimental

2.1. Materials and instruments

Polyvinylpyrrolidone (PVP, M_w ≈10,000 g/mol), cobalt nitrate hexahydrate ($Co(NO_3)_2 \cdot 6H_2O$), tetracycline hydrochloride ($C_{22}H_{24}N_2O_8 \cdot HCl$), and sodium borohydride ($NaBH_4$) were purchased from Sigma-Aldrich. C_{60} fullerene and 2-methylimidazole ($C_4H_6N_2$) were purchased from Alfa Aesar. Toluene (C_7H_8), 2-propanol (C_3H_8O), and zinc nitrate hexahydrate ($Zn(NO_3)_2 \cdot 6H_2O$) were supplied by Daejung Chemicals. The crystal structures of the nanomaterials and nanocomposites were determined using powder X-ray diffraction (XRD; D8 Advance, Bruker, Germany) with Cu Kα radiation at 40 kV and 40 mA in a 2θ range from 5 to 90°, with a scan speed of 0.2 s/step. The lattice vibrations of the samples were investigated using Raman spectroscopy (B&W Tek i-Raman Plus instrument, BWS465-532S, USA) with a 40 mW Nd:YAG laser (532 nm). The surfaces of the hybrid nanocomposites were examined using scanning electron microscopy (SEM; JSM-6510, JEOL Ltd., Japan) at a magnification of 10000 ~ 15000× and an accelerating voltage of 10 ~15 kV. The photocatalytic activity of the synthesized Co/Zn ZIF nanoparticles and Co/ZnZIF-C_{60} FNW composite in the degradation of TCH under LED light irradiation at 450 nm using UV–Vis spectrophotometry (Lambda 365, Perkin-Elmer, Germany). Ultrasonic irradiation was applied using an ultrasonic processor (VCX750, USA) with an output power of 750 W and a frequency of 20 kHz. The TCH solution was irradiated with visible light using LED (T5 Jinsung Electronic., Ltd), including a blue LED lamp (5 W, 450 nm).

2.2. Synthesis of bimetallic Co/Zn-ZIF nanoparticles

Cobalt nitrate hexahydrate (0.58 g) was dissolved in methanol (20 mL) and the mixture was stirred for 10 min. Similarly, zinc nitrate hexahydrate (0.48 g) was dissolved in methanol (20 mL) and stirred for 10 min. 2-methylimidazole (1.34 g) was dissolved in methanol (10 mL) and stirred for 10 min. The cobalt nitrate hexahydrate solution was gradually added to the zinc nitrate hexahydrate solution and stirred for 20 min. This mixture was gradually added to 2-methylimidazole solution, and the resulting mixture was stirred for 2 h. The solution was then stood at room temperature for 24 h and the precipitate was collected by centrifugation at 4000 rpm. The precipitate was then dispersed in methanol (10 mL) and sonicated for 4 h. The resulting suspension was further centrifuged at 4000 rpm to obtain the bimetallic CoZn-ZIF nanoparticles as a solid, which were dried in an oven at 70 °C for 24 h [33].

2.3. Synthesis of C_{60} fullerene nanowhiskers

The C_{60} fullerene (100 mg) was added to toluene (100 mL) in an Erlenmeyer flask, followed by stirring and ultrasonic treatment. The saturated C_{60} fullerene solution in toluene and isopropyl alcohol were then stored at 5 °C for 20 min before being mixed in a 50 mL vial. This mixed solution was subjected to ultrasonic treatment for 15 min and stored at 5 °C for 24 h before being filtered to obtain the solid product, which was dried in an oven for 2 h to obtain the desired compound.

2.4. Synthesis of hybrid Co/Zn-ZIF-C_{60} FNW composite

2-methylimidazole (1.34 g) was dissolved in methanol (10 mL) and stirred for 10 min. Separately, PVP (M_w ≈10,000 g/mol, 0.1 g) and C_{60} FNW (0.05 g) were dispersed in methanol (10 mL) and stirred for 10 min. Cobalt nitrate hexahydrate (0.58 g) and zinc nitrate hexahydrate (0.48 g) were dissolved in methanol (20 mL) and the mixture was stirred for 10 min. The C_{60} FNW solution and mixed metal nitrate solution were then gradually added to the 2-methylimidazole solution under stirring for 30 min. The resulting mixture was stirred for a further 2 h and then allowed to stand at room temperature for 24 h. The precipitate was collected by centrifugation at 4000 rpm and redispersed in methanol (10 mL), sonicated for 1 h, and further centrifuged at 4000 rpm to isolate the solid product. Finally, the product was dried in an oven at 70 °C for 24 h to yield the Co/Zn-ZIF-C_{60} FNW composite.

2.5. Photocatalytic activity and kinetics of bimetallic Co/Zn-ZIF nanoparticles and hybrid Co/Zn-ZIF-C_{60} FNW composite for TCH degradation under LED light

A TCH solution (1.0 mM) was prepared in distilled water (25 mL). Bimetallic Co/Zn ZIF nanoparticles (1 mg/mL) and the hybrid nanocomposite (1 mg/mL) were added to this aqueous solution, and stored in the dark conditions for 30 min to achieve an adsorption-desorption equilibrium between phtocatalysts and TCH. The reaction solution was subsequently irradiated with a 450 nm LED lamp at 15 min intervals. The maximum absorption of TCH was measured in the range of 365–380 nm using UV–Vis spectrophotometry.

3. Results and Discussion

3.1. Characterization of bimetallic Co/Zn-ZIF nanoparticles and hybrid Co/Zn-ZIF-C_{60} FNW composite

The XRD spectra of the bimetallic Co/Zn-ZIF nanoparticles (Fig. 1(a)) shows peaks at 7.31°, 10.34°, 12.69°, 14.67°, 16.41°, 18.04°, and 26.63° corresponding to the (011), (002), (112), (022), (013), (222), and (134) planes of the bimetallic Co/Zn-ZIF nanoparticles, respectively [33]. The spectrum of the hybrid Co/Zn-ZIF-C_{60} FNW composites (Fig. 1(b)) shows additional peaks at 10.79°, 17.70°, 20.74°, 28.07°, 30.86° and 32.78° corresponding to the (111), (220), (311), (420), (422), and (333) planes of the C_{60} FNW [29], while those at 7.38°, 10.42°, 12.77°, 14.75°, 16.49°, 18.07° and 26.71° correspond to the bimetallic Co/Zn-ZIF nanoparticles.

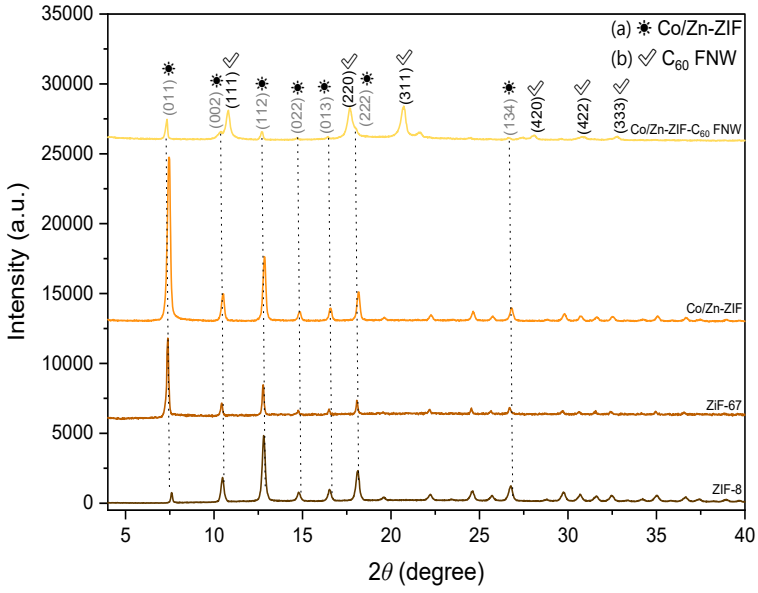

Fig. 1. XRD patterns of ZIF-8, ZIF-67, Co/Zn-ZIF nanoparticles and (a) Co/Zn-ZIF- (b) C_{60} FNW composite.

Table 1. Crystallite size of the Co/Zn ZIF nanoparticles (NPTs) in the Co/Zn ZIF-C_{60} FNW composite calculated using Sherrer's equation

Compound	Plane (h k l)	2 θ (degree)	Full Width at Half Maximum (degree)	Crystallite size (nm)
Co/Zn ZIF NPTs	011	7.38	0.10	77.30
	002	10.42	0.11	71.06
	112	12.77	0.12	64.80
	022	14.75	0.13	60.85
	013	16.49	0.12	65.36
	222	18.07	0.12	66.28
	134	26.71	0.15	55.76
Average				65.92

The peaks in the XRD spectrum of the bimetallic Co/Zn ZIF nanoparticles were slightly broader than those in the spectra of the monometallic ZIF-8 and ZIF-67 nanoparticles owing to the slight difference in the Co–N (1.976 Å) and Zn–N (1.987 Å) bond lengths, which induces local structural distortions and associated strain within the framework [34]. Furthermore, the XRD patterns demonstrate the high purity and crystallinity of the samples, confirming the successful synthesis of the hybrid Co/Zn-ZIF-C_{60} FNW composite. The mean crystallite size of the bimetallic Co/Zn-ZIF nanoparticles was calculated using Scherrer's equation, $D = k \cdot \lambda / \beta \cdot \cos\theta$, in which D is the crystallite size, λ is the wavelength of the Cu-Kα radiation (λ = 0.154178 nm), k is a shape factor (taken as 0.9), 2θ is the angle between the incident and scattered X-rays, and β is the full width at half maximum. The average crystallite size of the bimetallic Co/Zn-ZIF nanoparticles was 65.92 nm (Table 1).

The Raman spectrum of the hybrid Co/Zn-ZIF-C_{60} FNW composite (Fig. 2) exhibits peaks at 270 cm^{-1} (Hg (1)), 491 cm^{-1} (Ag (1)), and 1459 cm^{-1} (Ag (2)), demonstrating the presence of C_{60} FNW [29]. Additionally, the bands at 281 cm^{-1}, 428 cm^{-1} are likely attributable to the stretching vibrations of Zn-N and Co-N in the bimetallic Co/Zn-ZIF nanoparticles [35].

SEM images of the Co/Zn-ZIF (Fig. 3(a)) show the uniform rhombic dodecahedral morphology of the material, which is characteristic of metal-based ZIFs. The crystals of Co/Zn-ZIF were smaller than those of the monometallic ZIFs owing to the stress within the network. The Co/Zn-ZIF nanoparticles measured between 60–80 nm. The incorporation of Co and Zn into the same ZIF crystal likely induced local distortions, producing stress that inhibited crystal growth and thus resulted in smaller crystals in powder form

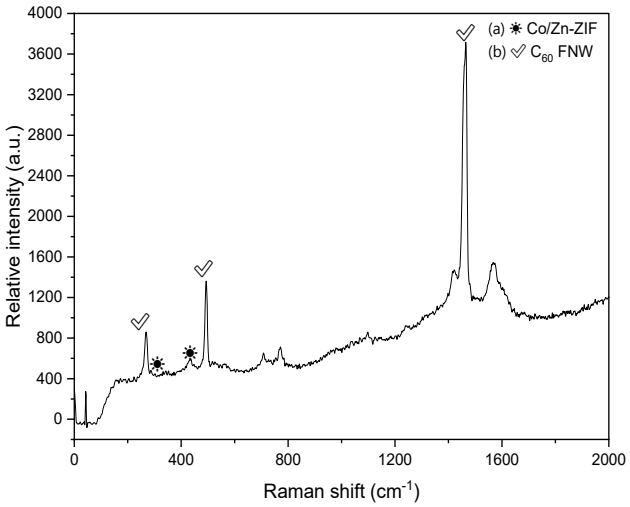

Fig. 2. Raman spectrum of (a) Co/Zn-ZIF- (b) C_{60} FNW composite.

[33]. Furthermore, the uniform rhombic dodecahedral Co/Zn-ZIF nanoparticles were distributed on the surface of the cylindrical structure of the C_{60} FNW (Fig. 3(b)).

In the hybrid Co/Zn ZIF-C_{60} FNW composite, Co/Zn-ZIF nanoparticles agglomerate by self-assembly on the surface of the one-dimensional C_{60} FNW due to the interaction of π-π stacking and van der Waals forces [36].

The Co/Zn-ZIF nanoparticles are deposited on the surface of the C_{60} FNW by physical adsorption through the LLIP method [37, 38].

The Co/Zn ZIF-C_{60} FNW composite used in this study was formed by a co-precipitation method.

In Fig. 3(b), the Co/Zn ZIF nanoparticles are placed surrounding the C_{60} FNW surface; therefore, the size of the length and diameter are larger than the original C_{60} FNW.

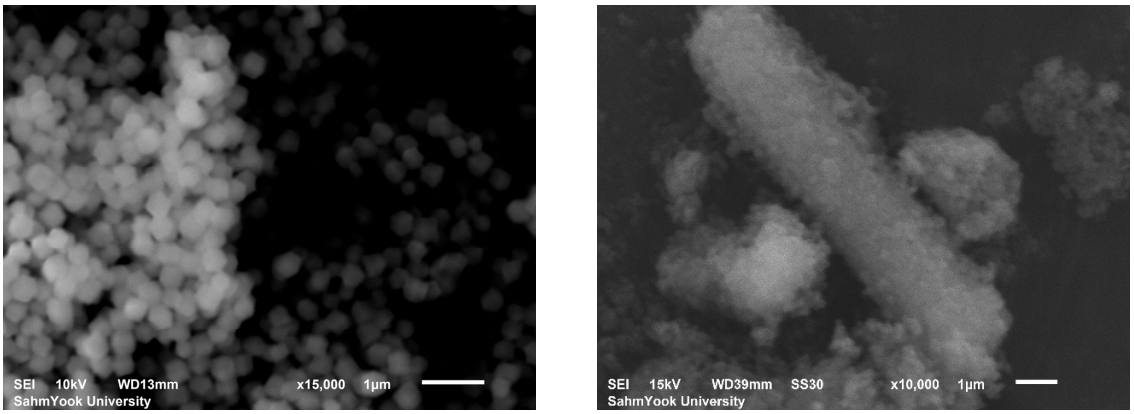

Fig. 3. SEM images of (a) Co/Zn-ZIF nanoparticles and (b) Co/Zn-ZIF-C_{60} FNW composite.

3.2. Tetracycline hydrochloride degradation using bimetallic Co/Zn-ZIF nanoparticles and hybrid Co/Zn-ZIF-C_{60} FNW composite under LED light irradiation: Photocatalytic activity and kinetics

The photocatalytic degradation of TCH using the bimetallic Co/Zn-ZIF nanoparticles and hybrid Co/Zn-ZIF-C_{60} FNW composite were monitored using UV-Vis spectrophotometry (Fig. 4). Also, because we have performed photocatalyst experiments after adsorption-desorption equilibrium was achieved for 30 min under dark conditions, the degradation of TCH was a photocatalytic reaction rather than a photolysis or adsorption reaction. The degradation rate D of the TCH solution was calculated using Eq. (1): [39, 40]

$$\text{TCH degradation (D)}\% = \frac{(A_0 - A_t)}{A_o} \times 100\% = \frac{(C_0 - C_t)}{C_0} \times 100\% \quad (1)$$

where A_0 and C_0 is the initial absorption and concentration of the TCH solution after adsorption-desorption equilibrium for 30 min, A_t and C_t is the absorption and concentration of TCH solution at time t. The degradation (D) of TCH in the presence of Co/Zn-ZIF nanoparticles reached 57.55% (A_0:1.0410, A_t:0.4419) upon irradiation at 450 nm for 120 min bimetallic (Fig. 4(a)). In contrast, a TCH degradation rate (D) of 68.10% (A_0:1.0230, A_t:0.3263) was observed in the presence of hybrid Co/Zn-ZIF-C_{60} FNW composite photocatalyst under identical conditions (Fig. 4(b)).

In the Co/Zn ZIF-C_{60} FNW composite as a photocatalyst, the role of C_{60} FNW enhanced suppression for recombination of electron-hole; therefore, photocatalytic activity for degradation of TCH is increased.

The reaction kinetics of the photocatalytic degradation of TCH using bimetallic Co/Zn-ZIF nanoparticles and the hybrid Co/Zn-ZIF-C_{60} FNW composite under LED light irradiation are shown in Fig. 5.

The kinetics of the first-order reaction were determined using Eq. (2): [41]

$$\ln(C / C_0) = -k_1 C \quad (2)$$

where k_1 is the rate constant, C_0 is the initial TCH concentration, and C is the TCH concentration at time t.

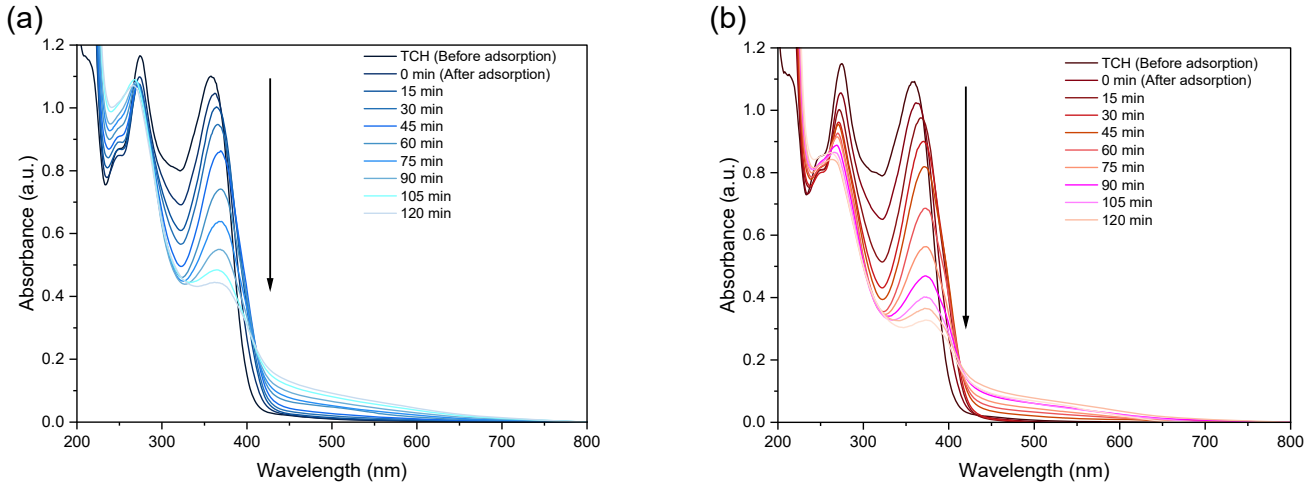

Fig. 4. UV-Vis spectra of TCH showing its photocatalytic degradation on (a) Co/Zn-ZIF nanoparticles and (b) Co/Zn-ZIF-C_{60} FNW composite under LED irradiation at 450 nm.

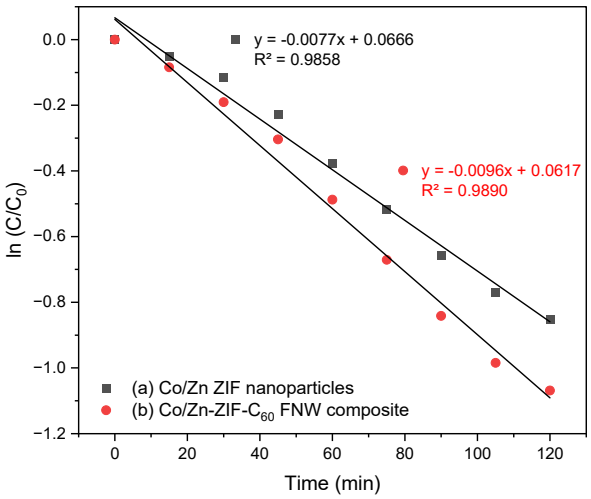

Fig. 5. Kinetics study of the photocatalytic degradation of TCH on (a) Co/Zn-ZIF nanoparticles and (b) Co/Zn-ZIF-C_{60} FNW composite under LED irradiation at 450 nm.

The photocatalytic degradation of TCH over the photocatalysts followed pseudo-first-order kinetics, as evidenced by the linearity of the reaction curves (Fig. 5). The coefficients of determination (R^2) of the pseudo-first-order reaction kinetics were 0.9858 and 0.9890 (Fig. 5 (a) and Fig. 5 (b)), respectively.

4. Conclusion

A hybrid Co/Zn-ZIF-C_{60} FNW composite was successfully synthesized from 2-methylimidazole, cobalt nitrate hexahydrate, zinc nitrate hexahydrate, polyvinylpyrrolidone (PVP, M_w ≈10,000 g/mol), and C_{60} FNW. The bimetallic Co/Zn-ZIF nanoparticles and hybrid Co/Zn-ZIF-C_{60} FNW composite were characterized using XRD spectroscopy, Raman spectroscopy, and SEM. The photocatalytic degradation of TCH under LED irradiation (at 450 nm) was performed using both the bimetallic Co/Zn-ZIF nanoparticles and the hybrid Co/Zn-ZIF-C_{60} FNW composite. The photocatalytic activity of the hybrid Co/Zn-ZIF-C_{60} FNW composite in the degradation of TCH was superior to that of the Co/Zn-ZIF nanoparticles. Moreover, the kinetics study for the photocatalytic degradation of TCH using both bimetallic Co/Zn-ZIF nanoparticles and the hybrid Co/Zn-ZIF-C_{60} FNW composite followed a pseudo-first order rate raw.

Acknowledgments

This study was supported by research funding from Sahmyook University in Korea.

References

[1]. A.A. Basheer, Chemical chiral pollution: Impact on the society and science and need of the regulations in the 21st century, *Chirality* 30 (2018) 402–406. DOI: 10.1002/chir.22808

[2]. Z.A. Alothman, A.Y. Badjah, O.M. Alharbi, I. Ali, Cobalt doping of titanium oxide nanoparticles for atenolol photodegradation in water, *Environ. Sci. Pollut. Res.* 28 (2021) 7423–7430. DOI: 10.1007/s11356-020-11071-w

[3]. R. El Asmar, A. Baalbaki, Z. Abou Khalil, et al., Iron-based metal organic framework MIL-88-A for the degradation of naproxen in water through persulfate activation, *Chem. Eng. J.* 405 (2021) 126701. DOI: 10.1016/j.cej.2020.126701

[4]. J. Hou, J. Lin, H. Fu, et al., Vitamin B_{12} derived CoCNx composite confined in SBA-15 as highly effective catalyst to activate peroxymonosulfate for naproxen degradation, *Chem. Eng. J.* 389 (2020) 124344. DOI: 10.1016/j.cej.2020.124344

[5]. N. Ahmadpour, M.H. Sayadi, S. Sobhani, M. Hajiani, A potential natural solar light active photocatalyst using magnetic $ZnFe_2O_4$@TiO_2/Cu nanocomposite as a high performance and recyclable platform for degradation of naproxen from aqueous solution, *J. Clean. Prod.* 268 (2020) 122023. DOI: 10.1016/j.jclepro.2020.122023

[6]. L. Feng, E.D. van Hullebusch, M.A. Rodrigo, et al., Removal of residual anti-inflammatory and analgesic pharmaceuticals from aqueous systems by electrochemical advanced oxidation processes. A review, *Chem. Eng. J.* 228 (2013) 944–964. DOI: 10.1016/j.cej.2013.05.061

[7]. R. Daghrir, P. Drogui, Tetracycline antibiotics in the environment: a review, *Environ. Chem. Lett.* 11 (2013) 209–227. DOI: 10.1007/s10311-013-0404-8

[8]. C. Gu, K.G. Karthikeyan, Interaction of Tetracycline with Aluminum and Iron Hydrous Oxides, *Environ. Sci. Technol.* 39 (2005) 2660–2667. DOI: 10.1021/es048603o

[9]. R. Pulicharla, K. Hegde, S.K. Brar, R.Y. Surampalli, Tetracyclines metal complexation: Significance and fate of mutual existence in the environment, *Environ. Pollut.* 221 (2017) 1–14. DOI: 10.1016/j.envpol.2016.12.017

[10]. G. Gopal, S.A. Alex, N. Chandrasekaran, A. Mukherjee, A review on tetracycline removal from aqueous systems by advanced treatment techniques, *RSC Adv.* 10 (2020) 27081–27095. DOI: 10.1039/D0RA04264A

[11]. A.C. Sophia, E.C. Lima, N. Allaudeen, S. Rajan,

Application of graphene based materials for adsorption of pharmaceutical traces from water and wastewater- a review, *Desalin. Water Treat.* 57 (2016) 27573–27586. DOI: 10.1080/19443994.2016.1172989

[12]. E.F. Polonio, J.F. Navarro, M.I.I. Clar, et al., Removal of pharmaceutical compounds commonly-found in wastewater through a hybrid biological and adsorption process, *J. Environ. Manag.* 263 (2020) 110368. DOI: 10.1016/j.jenvman.2020.110368

[13]. K. Kimura, H. Hara, Y. Watanabe, Removal of pharmaceutical compounds by submerged membrane bioreactors (MBRs), *Desalination* 178 (2005) 135–140. DOI: 10.1016/j.desal.2004.11.033

[14]. J. Zhong, X. Yuan, J. Xiong, et al., Solvent-dependent strategy to construct mesoporous Zr-based metal-organic frameworks for high-efficient adsorption of tetracycline, *Environ. Res.* 226 (2023) 115633. DOI: 10.1016/j.envres.2023.115633

[15]. Y. Jeganathan, T. Asharp, K. Nadarajah, Adsorptive behavior of engineered biochar /hydrochar for tetracycline removal from synthetic wastewater, *Environ. Pollut.* 345 (2024) 123452. DOI: 10.1016/j.envpol.2024.123452

[16]. M. Zhang, Y. Li, X. Zhou, et al., Preparation of ZIF-67/C_3N_4 composite material and adsorption of tetracycline hydrochloride, *Environ. Sci. Pollut. Res.* 30 (2023) 94112–94125. DOI: 10.1007/s11356-023-28919-6

[17]. Y. Shi, X. Wang, C. Feng, S. Yang, Nano-clay montmorillonite removes tetracycline in water: Factors and adsorption mechanism in aquatic environments, *iScience* 27 (2024) 108952. DOI: 10.1016/j.isci.2024.108952

[18]. L. Hao, X.L. Liu, J.T. Wang, et al., Metal-organic framework derived magnetic nanoporous carbon as an adsorbent for the magnetic solid-phase extraction of chlorophenols from mushroom sample, *Chin. Chem. Lett*. 27 (2016) 783–788. DOI: 10.1016/j.cclet.2016.01.021

[19]. Y. Liu, G. Zeng, L. Tang, et al., Highly effective adsorption of cationic and anionic dyes on magnetic Fe/Ni nanoparticles doped bimodal mesoporous carbon, *J. Colloid Interface Sci.* 448 (2015) 451–459. DOI: 10.1016/j.jcis.2015.02.037

[20]. A.L. Cazetta, O. Pezoti, K.C. Bedin, et al., Magnetic Activated Carbon Derived from Biomass Waste by Concurrent Synthesis: Efficient Adsorbent for Toxic Dyes, *ACS Sustain. Chem. Eng.* 4 (2016) 1058–1068. DOI: 10.1021/acssuschemeng.5b01141

[21]. K. Miyazawa, A. Obayashi, M. Kuwabara, C_{60} Nanowhiskers in a Mixture of Lead Zirconate Titanate Sol–C_{60} Toluene Solution, *J. Am. Ceram. Soc.* 84 (2001) 3037–3039. DOI: 10.1111/j.1151-2916.2001.tb01133.x

[22]. K. Miyazawa, M. Yoshitake, Y. Tanaka, Characterisation of platinum nanoparticles deposited on C_{60} fullerene nanowhiskers, *Surf. Eng.* 34 (2018) 846–851. DOI: 10.1080/02670844.2017.13967

[23]. K. Miyazawa, Synthesis of fullerene nanowhiskers using the liquid–liquid interfacial precipitation method and their mechanical, electrical and superconducting properties, *Sci. Technol. Adv. Mater.* 16 (2015) 013502. DOI: 10.1088/1468-6996/16/1/013502

[24]. R. Kato, K. Miyazawa, Raman Laser Polymerization of C_{60} Nanowhiskers, *J. Nanotechnol.* 2012 (2012) 101243. DOI: 10.1155/2012/101243

[25]. J.W. Ko, W.B. Ko, Catalytic Activity for Reduction of 4-Nitrophenol with [C_{60}] Fullerene Nanowhisker-Silver Nanoparticle Composites, *Mater. Trans.* 57 (2016) 2122–2126. DOI: 10.2320/matertrans.M2016214

[26]. J.W. Ko, W.B. Ko, Catalytic activity of C_{60} fullerene nanowhisker–zeolitic imidazolate framework-67 composite for reduction of 4-nitrophenol, *Fullerenes, Nanotubes and Carbon Nanostructures* 31 (2023) 61–67. DOI: 10.1080/1536383X.2022.2120476

[27]. S.W. Ko, H. Chung, Preparation of C_{60} Fullerene Nanowhisker–CuS Nanoparticle Composites and Photocatalyst for Rhodamine B Degradation under Blue Light Emitting Diode Irradiation, *Eurasian Chem.-Technol. J.* 25 (2023) 65–71. DOI: 10.18321/ectj1496

[28]. J.W. Ko, W.B. Ko, Synthesis of g-C_3N_4-C_{60} fullerene nanowhisker composites and its photocatalytic activity for degradation of rhodamine B, *Fullerenes, Nanotubes and Carbon Nanostructures* 30 (2022) 693–698. DOI: 10.1080/1536383X.2021.2008368

[29]. J.W. Ko, S.H. Park, W.B. Ko, Methylene blue degradation photocatalytic activity of C_{60} fullerene nanowhisker–ZnS:Mn-glycine composites, *Fullerenes, Nanotubes and Carbon Nanostructures* 30 (2022) 1116–1122. DOI: 10.1080/1536383X.2022.2075854

[30]. M.Y. Masoomi, A. Morsali, A. Dhakshinamoorthy, H. Garcia, Mixed-Metal MOFs: Unique Opportunities in Metal-Organic Framework (MOF) Functionality and Design, *Angew Chem. Int. Ed. Engl.* 58 (2019) 15188–15205. DOI: 10.1002/anie.201902229

[31]. L. Feng, K.Y. Wang, G.S. Day, H.C. Zhou, The chemistry of multi-component and hierarchical framework compounds, *Chem. Soc. Rev*. 48 (2019) 4823–4853. DOI: 10.1039/C9CS00250B

[32]. Y. Zhang, J. Wei, L. Xing, et al., Superoxide radical mediated persulfate activation by nitrogen doped bimetallic MOF (FeCo/N-MOF) for efficient tetracycline degradation, *Sep. Purif. Technol.* 282 (2022) 120124. DOI: 10.1016/j.seppur.2021.120124

[33]. T.N. Nguyen, H.P. Nguyen, T.H. Kim, S.W. Lee, Bimetallic Co/Zn-ZIF as an Efficient Photocatalyst for Degradation of Indigo Carmine, *Korean J. Mater. Res.* 28 (2018) 68–74. DOI: 10.3740/MRSK.2018.28.1.68

[34]. C. Sámano-Alonso, J. Hernández-Obregón, R. Cabrera, J.A.I. Díaz-Góngora, E. Reguera, Tuning the adsorption potential. Separation of aromatic hydrocarbons by cobalt and zinc zeolitic imidazolate frameworks, *Colloid. Surface. A* 506 (2016) 50–56. DOI: 10.1016/j.colsurfa.2016.06.008

[35]. Z. Öztürk, M. Filez, B. M. Weckhuysen, Decoding Nucleation and Growth of Zeolitic Imidazolate Framework Thin Films with Atomic Force Microscopy and Vibrational Spectroscopy, *Chem. - Eur. J.* 23 (2017) 10915–10924. DOI: 10.1002/chem.201702130

[36]. J. Han, H. Wu, H. Fan, et al., Tuning the Phase Composition of Metal–Organic Framework Membranes for Helium Separation through Incorporation of Fullerenes, *J. Am. Chem. Soc.* 145 (2023) 14793–14801. DOI: 10.1021/jacs.3c03362

[37]. A.V. Baskar, M.R. Benzigar, S.N. Talapaneni, et al., Self-Assembled Fullerene Nanostructures: Synthesis and Applications, *Adv. Funct. Mater*. 32 (2022) 2106924. DOI: 10.1002/adfm.202106924

[38]. B. Chai, X. Liao, F. Song, H. Zhou, Fullerene modified C_3N_4 composites with enhanced photocatalytic activity under visible light irradiation, *Dalton Trans.* 43 (2013) 982–989. DOI: 10.1039/C3DT52454J

[39]. G.H. Safari, M. Hoseini, M. Seyedsalehi, et al., Photocatalytic degradation of tetracycline using nanosized titanium dioxide in aqueous solution, *Int. J. Environ. Sci. Technol.* 12 (2015) 603–616. DOI: 10.1007/s13762-014-0706-9

[40]. L. Zhong, C. Wang, X. Cui, Use of mesoporous BiOI microspheres for sonocatalytic degradation of tetracycline hydrochloride, *Ecotoxicol. Environ. Saf.* 237 (2022) 113547. DOI: 10.1016/j.ecoenv.2022.113547

[41]. Y. Cao, X. Lei, Q. Chen, et al., Enhanced photocatalytic degradation of tetracycline hydrochloride by novel porous hollow cube $ZnFe_2O_4$, *J. Photochem. Photobiol. A Chem.* 364 (2018) 794–800. DOI: 10.1016/j.jphotochem.2018.07.023